Available online at www.sciencedirect.com

ScienceDirect

Advances in Space Research 61 (2018) 830–836

ADVANCES IN SPACE RESEARCH
(a COSPAR publication)

www.elsevier.com/locate/asr

Formation of polymer micro-agglomerations in ultralow-binder-content composite based on lunar soil simulant

Tzehan Chen [a], Brian J. Chow [b], Ying Zhong [a], Meng Wang [b], Rui Kou [b], Yu Qiao [a,b,*]

[a] *Program of Materials Science and Engineering, University of California – San Diego, La Jolla, CA 92093, USA*
[b] *Department of Structural Engineering, University of California – San Diego, La Jolla, CA 92093-0085, USA*

Received 9 August 2017; received in revised form 25 October 2017; accepted 27 October 2017
Available online 6 November 2017

Abstract

We report results from an experiment on high-pressure compaction of lunar soil simulant (LSS) mixed with 2–5 wt% polymer binder. The LSS grains can be strongly held together, forming an inorganic-organic monolith (IOM) with the flexural strength around 30–40 MPa. The compaction pressure, the number of loadings, the binder content, and the compaction duration are important factors. The LSS-based IOM remains strong from −200 °C to 130 °C, and is quite gas permeable.

Keywords: Binder content; Lunar regolith; Structural material; In-situ resource utilization

1. Introduction

In the next a few decades, building large-scale lunar bases and/or research facilities on the Moon will probably be one of major breakthroughs of manned or unmanned lunar exploration missions (Toklu, 2000). Previously, the study in this area was focused on the first-generation lunar habitats, by using lightweight alloys or composites (Happel, 1993; Khoshnevis et al., 2005). Since the distance from the Earth to the Moon is longer by three orders of magnitude than to the Low-Orbit International Space Station (ISS) (Kitmacher, 2010), with the limited space transportation capacity, if all the materials and components are transported from the Earth, the construction would be expensive and time consuming. It is, therefore, highly desirable that locally harvestable resources, such as lunar regolith, can be utilized (Benaroya, 2002).

A major component of lunar soil is silica. While, once heated to above 1200 °C, silica grains can be fused together, the thermal processing consumes a large amount of energy (Taylor and Meek, 2005). No low-melting-point salts or salts capable of lowering the melting point of silica, e.g. soda, have been discovered on the Moon (Schrader et al., 2010). Many other options, including production of cementitious materials (Beyer, 1985) and utilization of byproducts of lunar mining activities (Schrunk et al., 2007), demand sophisticated machinery and the final products may not survive the harsh lunar environment.

A promising concept is to bond lunar regolith grains by a small amount of binder. The binder should be lightweight, strong, and easy to handle. Some binder materials used on the Earth, such as sulfur (Meyers and Toutanji, 2007), are not compatible with the wide temperature range at lunar surface. Among all the materials — metals and alloys, ceramics, and polymers, high-temperature polymers, e.g. advanced epoxy, are attractive candidates.

Previously, we conducted research on JSC-1a lunar soil simulant (Qiao et al., 2007a), and fabricated lunar-soil-

---

* Corresponding author at: Department of Structural Engineering, University of California – San Diego, La Jolla, CA 92093, USA.
E-mail address: yqiao@ucsd.edu (Y. Qiao).

https://doi.org/10.1016/j.asr.2017.10.050
0273-1177/

simulant (LSS) based organic-inorganic monolith (IOM), using polyethylene (PE) or unsaturated polyester resin (UPR) as the binder (Chen et al., 2015a, 2015b, 2017). In an IOM, the organic binder holds together the inorganic LSS filler grains (Qiao et al., 2007b). The processing technique was similar to conventional compression molding. The experimental data demonstrated that LSS-based IOM could be stronger than typical steel-reinforced concrete.

In a regular compression molding procedure of particulate composite, full dispersion and wetting of polymer binder with filler particles is achieved prior to the compression, through extensive mixing. The binder content must be higher than 10–15 wt%; otherwise the mixture is too "dry", causing a high defect density (Figovsky and Beilin, 2013). In the work of Chen et al. (2017), we began with an initial binder content of 15 wt% and used a high densification pressure to squeeze out the redundant binder and to crush and close-pack the LSS filler grains. The lower limit of the binder content was 8.6 wt% (Fig. 1a). To minimize the burden on space transportation, we aim at an ultra-low binder content below 5 wt%. In order to reach this goal, major improvement must be made.

In Fig. 1a, not all the polymer phase is equally important. The portion of binder at the direct contact points among the filler grains is most critical, and the portion in the interior of interstitial sites does not directly contribute to the load-carrying capacity. A more efficient binder distribution is depicted in Fig. 1b. The binder forms polymer micro-agglomerations (PMA) that bridge the filler grains together; the free space among filler grains is empty. In such a configuration, all the binder is utilized to carry load, and the binder content may reach a much lower level. For an order-of-magnitude assessment of the theoretical lower limit of binder content, we assume that the PMA size is ~1/5 of the size of interstitial site and the PMA form an ideal body center cubic (BCC) structure. The total PMA volume would be only ~1/60 of the free space. With this perfect PMA structure, the binder content can be reduced by ~60 times from that of Fig. 1a, to around 0.15 wt%.

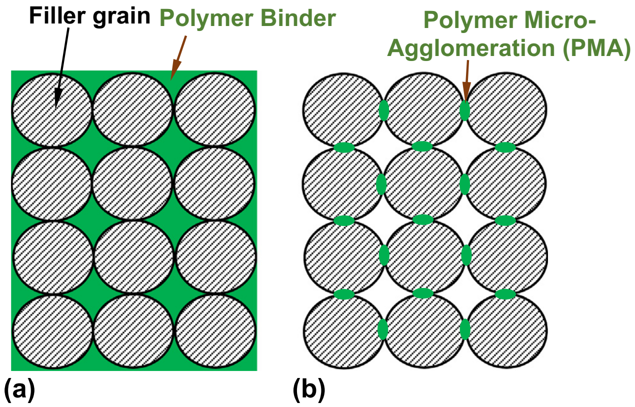

Fig. 1. Schematics of (a) close-packed filler grains, with the interstitial space being filled by ~8.6 wt% binder; and (b) polymer micro-agglomerations (PMA) that bridge the filler grains together, with the interstitial space being empty.

2. Experimental

In the current study, the filler was JSC-1a lunar soil simulant obtained from Orbitec. JSC-1a was upgraded from JSC-1 lunar soil simulant, with the composition and grain size and shape similar to those of Apollo lunar soil samples; it has been commonly accepted for lunar scientific research (e.g. McKay et al., 1994). The binder was Epon-828 epoxy resin provided by Miller-Stephenson, with the hardener being m-Xylylenediamine from Sigma-Aldrich. First, the epoxy resin and the hardener were mixed thoroughly, with the mass ratio of 5:1. Then, a small amount of epoxy-hardener mixture was dropped onto ~5 g of air-dried JSC-1a LSS filler grains (Fig. 2a). The binder content ranged from 2 wt% to 8 wt%. In a 50-ml beaker, the filler and the binder was mixed by a spatula for 5 min, and transferred to a stainless steel cylinder (Fig. 2b). The height of the steel cylinder was 50.8 mm and the inner diameter was 19.1 mm. The cylinder was capped from the top and the bottom by two stainless steel pistons, respectively. The piston diameter was 19.0 mm, loosely fitting with the inner surface of the steel cylinder. The filler-binder mixture was quasi-statically compacted by a type-5582 Instron machine, with the loading rate of 0.3 mm/min. The maximum compaction pressure, P_{max}, ranged from 20 MPa to 350 MPa. The maximum pressure was maintained for 1 min, and the piston was fully unloaded with an unloading rate of ~0.3 mm/min.

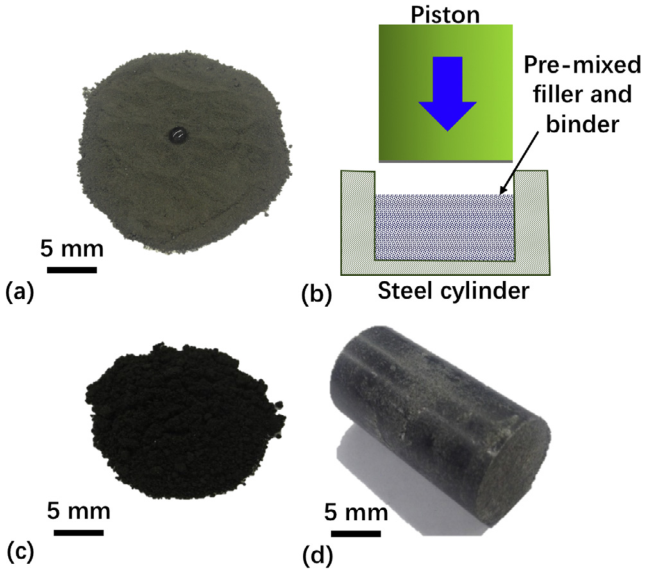

Fig. 2. (a) Photo of 4 wt% binder dropped onto ~5 g of air dried JSC-1a simulant filler. (b) Schematic of the compaction setup, wherein pre-mixed simulant-binder mixture is compressed by a steel piston in a steel cylinder. (c) Simulant-binder mixture after the first loading, which has been taken out of the steel cylinder and broken apart. (d) After the second loading and curing, the hardened IOM sample is taken out of the steel cylinder.

After the first loading, the top piston was removed and the compacted material was transferred out of the steel cylinder. Large aggregations of JSC-1a grains were broken apart by a lab spatula into small pieces with the size below 100 μm (Fig. 2c), and placed back into the steel cylinder. The mixture was compressed again through a similar procedure; the compression duration at $P_{\max}$ ranged from 1 min to 1 h. Then, while being kept in the steel cylinder, the compacted material was moved into a VWR-1330GM box furnace and the binder was cured at 100 °C for one hour in air. The cured IOM sample was cylindrical (Fig. 2d); it was cut by a MTI diamond saw into beam samples, and all the surfaces were polished by 320-grit sandpapers.

For some samples, the initial JSC-1a filler grain size distribution was controlled precisely. In a Tyler Ro-Tap 8-Inch Sieve Analyzer, air-dried JSC-1a grains were separated into different groups according to the mesh sizes of sieve trays. Some samples had random initial filler grain size distribution; some samples had relatively uniform initial filler grain size ~500 μm; some samples had two-stepped initial filler grain size distribution. The two-stepped grain size gradation was produced by mixing two groups of sieved JSC-1a grains that had the grain sizes between 90–112 μm and 20–25 μm, respectively; the mass ratio was 765:235.

Three-point bending test was carried out to measure the flexure strength of cured IOM:

$$R = (3/2)(F_{\max}L/bd^2) \tag{1}$$

where $F_{\max}$ is the maximum load and b, L, and d are the width, length, and height of the beam sample, respectively (Wight, 2002). The beam sample was simply supported at both ends, as depicted by the inset in Fig. 3. The measurement was conducted at various temperatures in the range between −200 °C and 130 °C, the expected temperatures range on lunar surface. For temperature higher than room temperature, the IOM sample was heated in an oven in air for 20 min. Low temperature was achieved by a bath of mixture of liquid nitrogen and alcohol; the sample was immersed in the bath for 20 min. Immediately after heating or cooling, the sample was tested in the Instron machine with the three-point bending setup.

Gas permeability of IOM samples was measured as

$$\kappa = v\mu \cdot \Delta x/\Delta P \tag{2}$$

where v is the gas flow rate, μ is the dynamic viscosity, Δx is the diffusion thickness, and ΔP is the pressure (McClintock and Argon, 1966). Compressed nitrogen was forced to flow through a disk-shaped IOM sample. The IOM sample was firmly held inside a polyurethane tube; the tube connected the compressed nitrogen tank to a water bath. The gas passing through the IOM sample was collected by an empty tube above the water bath and its volume was recorded as a function of time.

3. Results and discussion

Figs. 4–7 show our measurement results of flexural strength, R, of cured IOM samples. Fig. 8 shows the measured permeability as a function of the binder content, C. The fracture surfaces of tested IOM samples were observed under electron scanning microscope (SEM). Figs. 9–11 show typical SEM images.

With the low binder content, prior to compaction, the JSC-1a grains and the binder are non-uniformly mixed. Even after prolonged mixing, the mixture is sandy. As shown in Fig. 9a, binder drops larger than a few hundred μm attract small JSC-1a filler grains; little binder is attached to the largest filler grains. Such a structure contains many large-sized defects, and its structural integrity is poor. Fig. 2b describes the compaction operation: The pre-mixed simulant filler and binder are placed in a steel cylinder, and compressed quasi-statically by a steel piston. After the first compaction loading, the filler-binder mixture is taken out of the steel cylinder and broken apart into small pieces (Fig. 2c). Fig. 9b shows that the distribution of binder becomes more uniform. The largest binder drops are dispersed into small droplets, and the clusters of small filler grains are disrupted. Large filler grains are crushed,

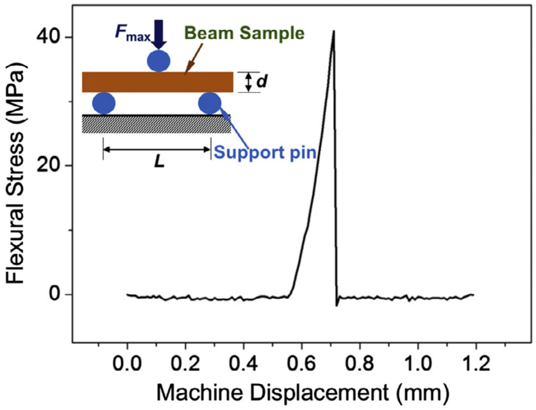

Fig. 3. A Typical load-displacement curve of flexure strength measurement. The inset at the upper-left corner depicts the experimental setup.

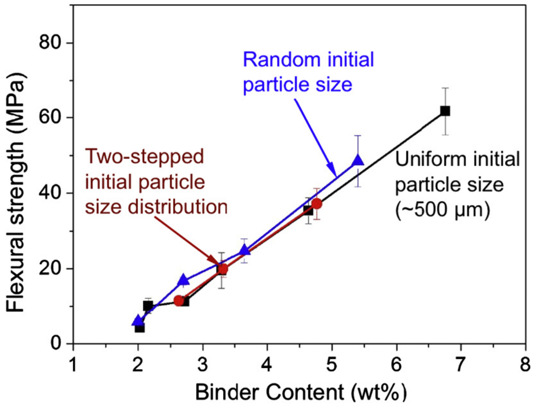

Fig. 4. The flexural strength (R) of LSS-based IOM with various initial grain size distributions.

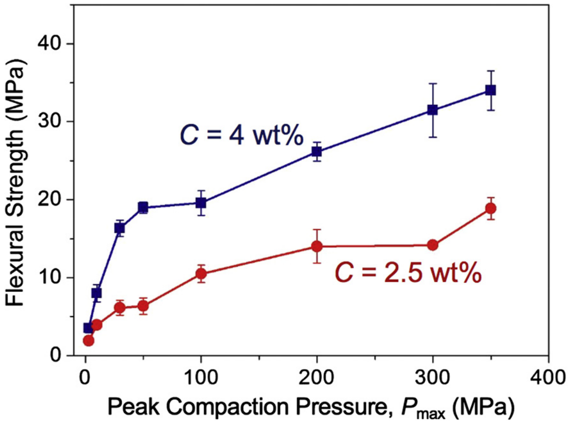

Fig. 5. The flexural strength (*R*) of LSS-based IOM as a function of the maximum compaction pressure (P_{max}). The compression duration is 1 min.

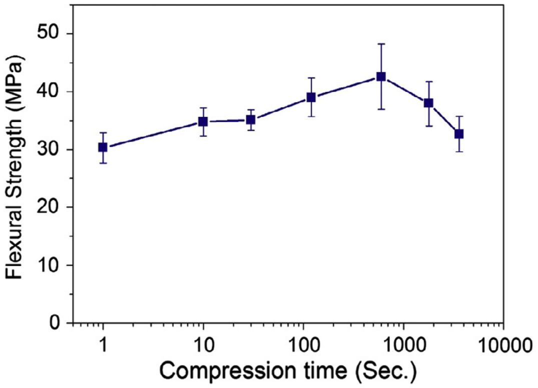

Fig. 6. The flexural strength (*R*) of LSS-based IOM as a function of the compression duration. The binder content (*C*) is 4 wt% and the maximum compaction pressure (P_{max}) is 350 MPa.

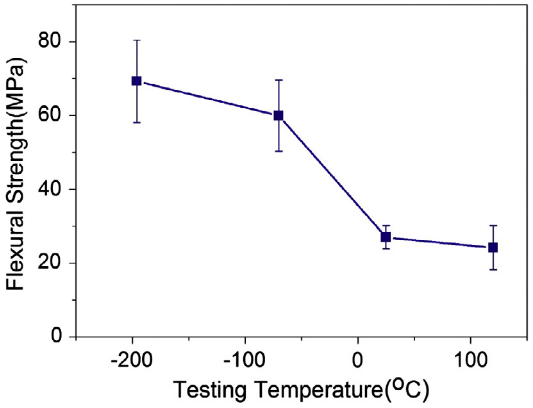

Fig. 7. The flexural strength (*R*) of LSS-based IOM at various testing temperatures.

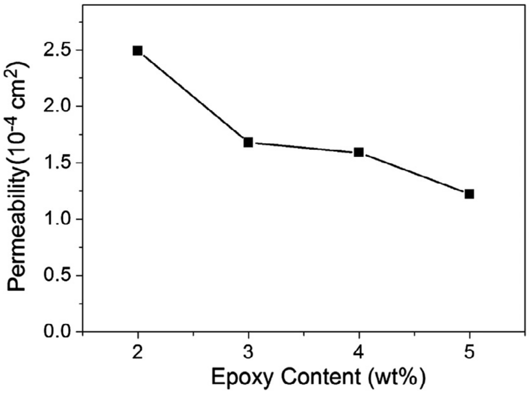

Fig. 8. Permeability of LSS-based IOM with various binder contents. The maximum compaction pressure is 350 MPa; the compression duration is 1 min.

and form a close-packed configuration with smaller JSC-1a filler pieces. Fig. 9c is an example of initially large filler grain, crushed into a few smaller pieces and bridged together by binder droplets. However, relatively large binder drops and poorly wetted filler grains can still be observed (Fig. 9d); they would lead to defects, causing relatively low material strength.

The filler gains and the binder are much better mixed after the second compaction (Fig. 10a). The compaction pressure and loading rate are identical to those of the first loading. When the maximum compaction pressure (P_{max}) is 350 MPa, no evident defects can be found in the cured IOM sample; the binder exists as small-sized polymer micro-agglomerations (PMA) around the contact points among simulant grains. When P_{max} is lower, Fig. 10b and c indicate that the binder dispersion is incomplete. When P_{max} is 100 MPa, a large number of loosely attached filler grains can be observed; when P_{max} is 30 MPa, the binder distribution pattern is somewhat similar to that of non-compressed mixture. Clearly, repeated high-pressure compaction helps break apart the initially large binder drops, as the filler grains are compacted toward each other and "squeeze" the binder phase over a large area of grain surfaces (Fig. 12a). When the compaction pressure rises, the dispersed binder is driven by the large capillary force in the narrowest "channels" and is self-assembled to the contact points of adjacent filler grains (Fig. 12b), resulting in the PMA configuration (Fig. 1b). As the interstitial space is procedurally left empty, the separated PMA form a network that carries external load. If P_{max} is low, the capillary pressure would be insufficient, as the filler grains are not closely compressed and the space among them is relatively wide. After the second compression, further increasing the number of loadings does not lead to much improvement in flexural strength.

With appropriate compaction and curing, the IOM samples are quite strong, as shown in Fig. 3. The bending force increases linearly with the deflection, and at F_{max} brittle failure takes place. The final fracture always begins at the center point of the bottom surface of the IOM beam sample. When the binder content (*C*) is only 2 wt%, Fig. 11a suggests that there are relatively large number of defects in the cured IOM sample. When *C* is ~10 wt%, Fig. 11b

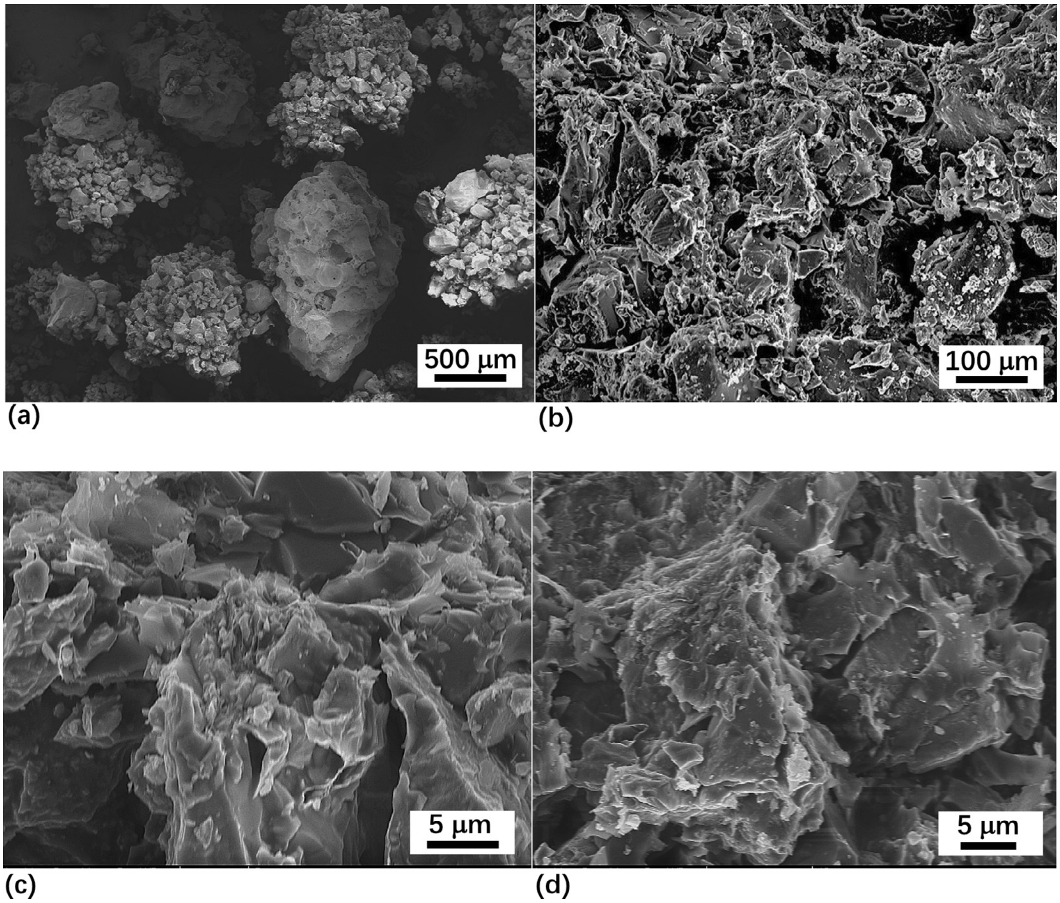

Fig. 9. (a) Simulant-binder mixture prior to the first loading. (b) Simulant-binder mixture after the first loading, and its local view fields showing (c) crushed simulant grains bridged by binder droplets and (d) large binder droplets. The compaction pressure is 350 MPa; the compression duration is 1 min; the initial simulant grain size distribution is random; the binder content is 3.3 wt%.

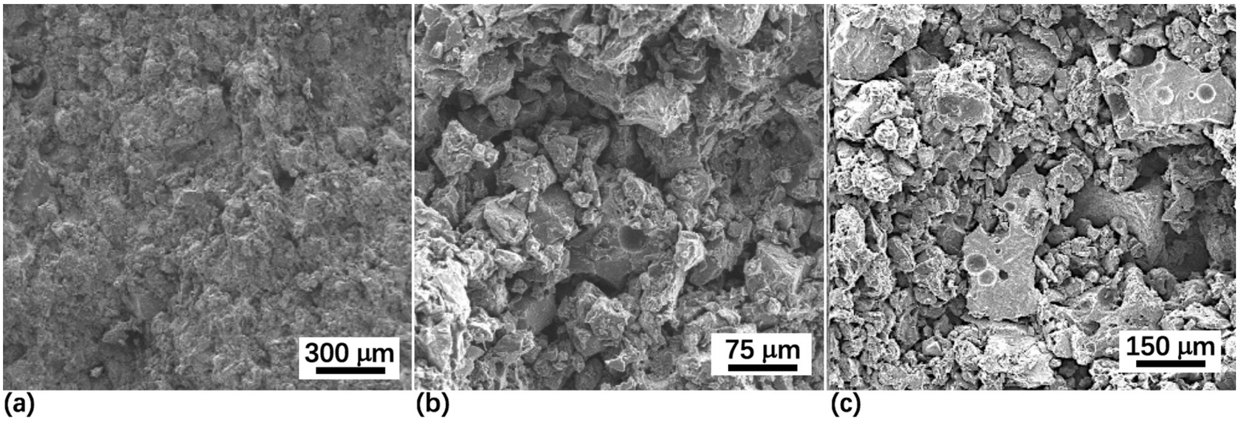

Fig. 10. SEM images of IOM samples after the second loading, with the compaction pressures being (a) 350 MPa, (b) 100 MPa, and (c) 30 MPa, respectively. The compression duration is 1 min; the binder content is 3.3 wt%; the initial simulant grain size distribution is random.

suggests that not only most of the filler grains are bonded together, but also semi-continuous binder strips begin to show up; that is, excess binder tends to fill the interstitial space among filler grains. This observation is consistent with the flexural strength measurement results in Fig. 4. In the range of C from 2 wt% to 7 wt%, R is nearly linear to C. When $C = 2$ wt%, R is ~6 MPa, comparable with that of typical unreinforced portland cement (Wight, 2002); when $C = 3$ wt%; R is 15–20 MPa, comparable with that of typical steel-reinforced concrete (Wight, 2002); with $C = 4$ wt%, R is around 30 MPa; and as $C > 5$ wt%, R is around 50–60 MPa, comparable with those of many cast copper alloys (McClintock and Argon, 1966). Note that the initial filler grain size distribution does not have a pro-

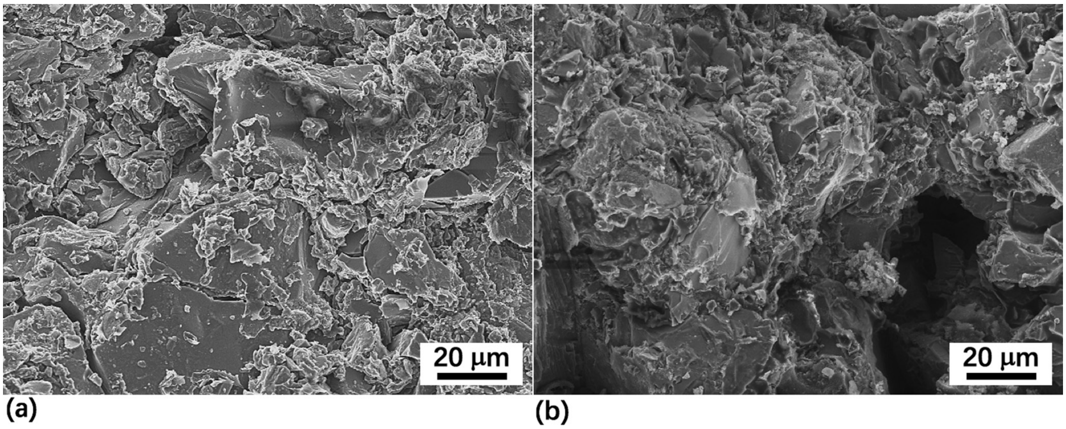

Fig. 11. SEM images of IOM samples after the second loading, with the binder contents of (a) 2 wt% and (b) 10 wt%, respectively. The compaction pressure is 350 MPa; the compression duration is 1 min; the initial simulant grain size distribution is random.

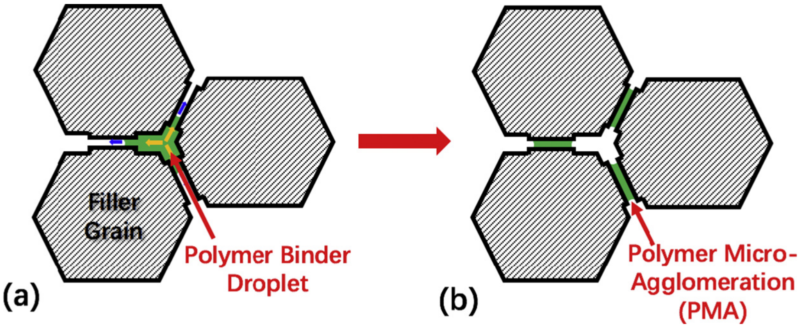

Fig. 12. Schematic of the compaction process: (a) A binder droplet is squeezed in the interstitial site among filler grains; (b) the binder is further driven into the narrowest space around the direct contact points among filler grains, by the large capillary force.

nounced influence on the IOM strength, since under the high compaction pressure the filler grains are crushed and therefore, the final grain size distribution is independent of the initial setting.

Fig. 5 shows the effects of compaction pressure (P_{max}) and binder content (C). The flexural strength is trivial at a low compaction pressure, and increases rapidly with P_{max} when P_{max} is less than 50 MPa; as $P_{max} > 50$ MPa, R increases relatively slowly; when $P_{max} > 350$ MPa, the influence of P_{max} becomes secondary. For the testing conditions in the current study, the optimum pressure is 200–350 MPa. The crushing strength of JSC-1a filler grains is measured as 20–30 MPa. It is clear that filler crushing must be achieved; otherwise the binder dispersion would not be promoted. From 50 to 350 MPa, the gain in flexural strength from the increase in compaction pressure may be attributed to the capillary flow depicted in Fig. 12b, which accounts for ~40% of total strength at $P_{max} = 350$ MPa.

The PMA formation takes time. As shown in Fig. 6, when the compression loading is maintained at P_{max} for a longer period time but below 10 min, R rises with the compaction duration (τ). When $C = 4$ wt%, the IOM sample obtains ~3/4 of its full strength immediately after the loading is applied, when τ is less than 1 s; the rest ~1/4 of strength is obtained as τ increases to 10 min. When $\tau > 10$ min, its increase causes a reduction in R, which is probably related to the setting of binder. If the binder begins to solidify before compression completes, the change in micro-configuration would result in defects in the binder phase and at the binder-filler interface. The measured R-τ relationship confirms that there exist two mechanisms of binder dispersion (Fig. 12). The first mechanism, which dominates short-term mixture behavior, may be associated with the flow of pressurized resin through the filler grain gaps. Due to the small length scale of filler grains, the viscous flow completes in less than 1 s. The second mechanism may be based on the capillary flow of resin along filler grain surfaces, toward the narrowest space around contact points. The typical diffusion rate in a micron-sized channel of a viscous resin is on the scale of 10^{-4} m/s (Springer, 1982); the crushed filler grain size is around 10–100 μm. It takes a few to 10 min for the capillary surface diffusion to cover the entire filler grain, fitting well with the measured time scale in Fig. 6.

In the expected temperature range from −200 °C to 130 °C on lunar surface, satisfactory IOM strength is obtained (Fig. 7). The epoxy binder does not significantly soften when temperature is less than 130 °C, and its low-temperature strength is higher (Pascault et al., 2002).

The IOM samples are quite permeable to gas (Fig. 8). When the binder content is 2–5 wt%, the permeability of IOM is $1–2.5 \cdot 10^{-4}$ cm^2 s^{-1}, higher than that of typical portland cement by nearly two orders of magnitude, comparable with sorted gravel (Bear, 2013); the lower the binder content, the more permeable the IOM sample would be. That is, as *C* decreases, more interstitial sites among filler grains are empty, and vice versa.

The current study provides an approach for producing structural materials based on locally harvestable resources on lunar surface, with a relatively small amount of binder from the Earth. It may work together with other in-situ resource utilization concepts, such as sintering of lunar soils (Taylor and Meek, 2005) and lunar regolith geopolymers (e.g. Montes et al., 2015; Davis et al., 2017). Future development of IOM includes scaling up of materials processing as well as characterization of long-term materials performance in vacuum and upon intense radiation.

4. Concluding remarks

Lunar soil simulant (LSS) based inorganic-organic monolith (IOM) are processed through a specifically developed repeated-compaction technique, wherein pre-mixed LSS grains and a small amount of polymer binder are compacted quasi-statically. With a low binder content of only 2 wt% to 5 wt%, the flexural strength of IOM is comparable with or higher than that of typical steel-reinforced concrete. The maximum compaction pressure ($P_{\max}$) must be higher than the crushing strength of filler grains, so that close-packed configuration can be achieved and large binder drops are broken apart. As $P_{\max}$ further increases, the large capillary force promotes surface diffusion of binder around the contact points of filler grains, which forms polymer micro-agglomerations (PMA). Under the high compaction pressure, the pressurized flow of binder can be finished in less than 1 s.; the capillary flow takes a few to 10 min. The flexural strength increases quite linearly with the binder content, and tends to saturate when the binder content exceeds 10 wt%. The IOM strength is satisfactory when temperature is below 130 °C. The IOM is gas-permeable. This technology not only is useful to lunar construction materials, but also may be applied to terrestrial sands/soils or other planetary materials.

Acknowledgment

This work was supported by the National Aeronautics and Space Administration (NASA) under Grant No. NNX12AI73G, for which we are grateful to Dr. Robert A. Fogel.

References

Bear, J., 2013. Dynamics of Fluids in Porous Media. Courier, New York.

Benaroya, H., 2002. An overview of lunar base structures: past and future. In: AIAA Space Architecture Symp., October 10–11, Houston, TX, USA, pp. 10.

Beyer, L.A., 1985. Lunarcrete — a novel approach to extraterrestrial construction. In: Faughnan, B., Maryniak, G. (Eds.), Space Manufacturing 5: Engineering with Lunar and Asterodial Materials – Proc. 7th Princeton/AIAA/SSI Conf., New York, NY, p. 172.

Chen, T., Chow, B.J., Wang, M., Shi, Y., Zhao, C., Qiao, Y., 2015a. Inorganic-organic hybrid of lunar soil simulant and polyethylene. ASCE J. Mater. Civil Eng. 28 (4), 06015013.

Chen, T., Chow, B.J., Qiao, Y., 2015b. Two-step gradation of particle size in an inorganic-organic hybrid. Sci. Eng. Compos. Mater. 22, 643–647.

Chen, T., Chow, B.J., Wang, M., Zhong, Y., Qiao, Y., 2017. High-pressure densification of composite "lunar cement". ASCE J. Mater. Civil Eng. 29, 06017013.

Davis, G., Montes, C., Eklund, S., 2017. Preparation of lunar regolith based geopolymer cement under heat and vacuum. Adv. Space Res. 59, 1872–1885.

Figovsky, O., Beilin, D., 2013. Advanced Polymer Concretes and Compounds. CRC Press, Boca Raton, FL.

Happel, J.A., 1993. Indigenous materials for lunar construction. Appl. Mech. Rev. 46 (6), 313.

Khoshnevis, B., Bodiford, M.P., Burks, K.H., Ethridge, E., Tucker, D., Kim, W., Toutanji, H., Fiske, M.R., 2005. Lunar contour crafting - a novel technique for ISRU-based habitat development. In: 43rd AIAA Aerospace Sciences Meeting and Exhibit, Reno, NV, USA, pp. 7397.

Kitmacher, G.H., 2010. Reference Guide to the International Space Station. CreateSpace Independent Publ.

McClintock, M.F., Argon, A.S., 1966. Mechanical Behavior of Materials. Addison-Wesley, Boston.

McKay, D.S., Carter, J.L., Boles, W.W., Allen, C.C., Allton, J.H., 1994. JSC-1: a new lunar soil simulant. In: Galloway, R.G., Lokaj, S. (Eds.), Engineering, Construction, and Operations in Space IV, ASCE, pp. 875.

Meyers, C., Toutanji, H., 2007. Analysis of lunar-habitat structure using waterless concrete and tension glass fibers. J. Aerospace Eng. 20 (4), 220.

Montes, C., Broussard, K., Gongre, M., Simicevic, N., Mejia, J., Tham, J., Allouche, E., Davis, G., 2015. Evaluation of lunar regolith geopolymer binder as a radioactive shielding material for space exploration applications. Adv. Space Res. 56, 1212–1221.

Pascault, J.P., Sautereau, H., Verdu, J., Williams, R.J., 2002. Thermosetting Polymers. CRC Press, Boca Rton, FL.

Qiao, Y., Chen, J., Han, A., 2007a. An organic-inorganic nanohybrid based on lunar soil simulant. Adv. Eng. Mater. 9 (4), 325.

Qiao, Y., Chen, J., Han, A., Deliwala, J.K., 2007b. A simplified processing technique of organic–inorganic intercalation/exfoliation nanohybrid. Mater. Res. Bull. 42 (7), 1332.

Schrader, C., Rickman, D., McLemore, C., Fikes, J., 2010. Lunar Regolith Simulant User's Guide. NASA Report No. NASA/TM-2010-216446.

Schrunk, D., Sharpe, B., Cooper, B.L., Thangavelu, M., 2007. The Moon: Resources, Future Development and Settlement. Springer.

Springer, G.S., 1982. Resin flow during the cure of fiber reinforced composites. J. Comput. Mater. 16 (5), 400.

Taylor, L.A., Meek, T.T., 2005. Microwave sintering of lunar soil: properties, theory, and practice. J. Aerospace Eng. 18 (3), 188.

Toklu, Y.C., 2000. Civil engineering in the design and construction of a lunar base. In: Seventh International Conference and Exposition on Engineering, Construction, Operations, and Business in Space, February 27-March 2, Albuquerque, NM, USA, pp. 822.

Wight, J.K., 2002. Reinforced Concrete: Mechanics and Design. Pearson, New York.